Journal of Statistical Physics, Vol. 101, Nos. 1/2, 2000

Microscopic Chaos and Reaction-Diffusion Processes in the Periodic Lorentz Gas[1]

I. Claus[2, 3] and P. Gaspard[2]

Received November 5, 1999

We apply the hypothesis of microscopic chaos to diffusion-controlled reaction which we study in a reactive periodic Lorentz gas. The relaxation rate of the reactive eigenmodes is obtained as eigenvalue of the Frobenius–Perron operator, which determines the reaction rate. The cumulative functions of the eigenstates of the Frobenius–Perron operator are shown to be generalizations of Lebesgue's singular continuous functions. For small enough densities of catalysts, the reaction is controlled by the diffusion. A random-walk model of this diffusion-controlled reaction process is presented, which is used to study the dependence of the reaction rate on the density of catalysts.

KEY WORDS: Dynamical chaos; reactive Lorentz gas; reaction rate; isomerization; Frobenius–Perron operator; Poincaré–Birkhoff map; Pollicott–Ruelle resonances; Lebesgue singular function; random-walk; diffusion-controlled reaction; cross-diffusion.

1. INTRODUCTION

Reactive processes are of prime importance in many problems of current preoccupation in chemistry and physics such as pattern formation in non-equilibrium systems and in morphogenesis,[(1)] heterogeneous catalysis,[(2)] recombination processes in solid or liquid phases,[(3–5)] as well as high-energy reactions in astrophysical systems.[(6)] Yet, few studies have been devoted to the microscopic understanding of reactive processes. In this context, Nicolis and coworkers have carried out a study of an isomerization

[1] This paper is dedicated to Professor Grégoire Nicolis on the occasion of his sixtieth birthday.

[2] Center for Nonlinear Phenomena and Complex Systems, Faculté des Sciences, Université Libre de Bruxelles, Campus Plaine, Code Postal 231, B-1050 Brussels, Belgium.

[3] Aspirant FNRS.

0022-4715/00/1000-0161$18.00/0

kinetics induced by color exchange between the freely moving particles of an infinite one-dimensional ideal gas.[7–9] For this non-diffusive system, a reaction-diffusion equation was rigorously derived for the color density by Nicolis and coworkers.[8, 9] The diffusion-reaction equations for both the total and the color densities were later derived in the case of a related hard-rod gas model.[10] These one-dimensional systems have a surface dynamical randomness characterized by an infinite Kolmogorov–Sinai entropy per unit time which has its origin in the flux of particles continuously arriving from infinity with random positions and velocities distributed according to an equilibrium thermal distribution. However, in typical two- or three-dimensional systems, the dominant source of dynamical randomness is the local dynamical instability due to the defocusing character of the collisions between the particles and the question arises whether such a bulk dynamical randomness has a role to play in the justification of the macroscopic laws of kinetics. Already, relationships have been established between the transport coefficients and the characteristic quantities of chaos within the escape-rate formalism.[11–13] On the other hand, for chaotic systems, the hydrodynamic modes of diffusion have been explicitly constructed as singular eigenstates of the Liouvillian formalism, which justifies the exponential relaxation toward the thermodynamic equilibrium by chaotic diffusion.

Inspired by the pioneering work of Nicolis and coworkers, a study of isomerization kinetics in dynamical systems with a local dynamical instability has been recently undertaken in order to understand how the law of chemical kinetics can be derived from the microscopic chaotic dynamics.[14–16] A previous work has been devoted to a reactive multibaker model in which a colored particle undergoes a deterministic motion of diffusion induced by a bakertype chaotic mapping in a chain of squares.[15, 16] In this model, the color A or B changes when the particle passes by each one of the catalysts, which are a few special squares periodically distributed among the squares of the chain. For this model, the total density is governed by a diffusion equation and the color density by a reaction-diffusion equation if the spatial scales are large enough. The exponential relaxation toward equilibrium was characterized in terms of the Pollicott–Ruelle resonances[17, 18] of the Frobenius–Perron operator of the model, giving a full justification of the macroscopic laws of kinetics.

The purpose of the present paper is to extend the previous study to a more realistic model which is a reactive Lorentz gas on a two-dimensional periodic lattice. In this model, a colored particle moves in free flight between elastic collisions on fixed hard disks forming a triangular lattice. Its dynamics is known to be fully chaotic since the work by Bunimovich, Chernov and Sinai who proved that diffusion is normal when the horizon

is finite, i.e., when the disks are close enough to avoid infinite free flight along special directions of the lattice.[19, 20] In the present paper, we consider a reversible reactive process induced by the chaotic motion. Like in the reactive multibaker mapping, the particle carries a color A or B which changes instantaneously, and with a certain probability when the particle collides with a "catalyst" which is one of a few special disks periodically chosen among all the disks. The moving particle keeps its color upon collision on all the other disks. The kinetic scheme is thus

$$\begin{aligned} A + \text{catalytic disk} &\leftrightarrow B + \text{catalytic disk}, \qquad \text{with probability } p_0 \\ A + \text{other disk} &\leftrightarrow A + \text{other disk} \\ B + \text{other disk} &\leftrightarrow B + \text{other disk} \end{aligned} \tag{1}$$

Because of the probability of reaction, our model contains an extra source of dynamical randomness than the chaotic dynamics. The reactive process is deterministic only if the probability p_0 is set equal to unity. This *a priori* randomness of the reactive process is introduced to model the effect of a complex color dynamics on a reactive time scale which is shorter than the intercollisional time. We remark that one of the specificities of our model is that the reaction is a reversible isomerization. This reactive process differs from the standard process of von Smoluchowski where the particle is irreversibly absorbed by some reactive sinks.[3, 21, 22] Indeed, in the reversible isomerization process, the total number of particles is constant and the system is expected to reach an equilibrium where each color is equally distributed on the particles of the gas.

Our aim is to infer the macroscopic laws of chemical kinetics ruling the approach to the thermodynamic equilibrium from the chaotic dynamics of this model. For this purpose, we construct the Frobenius–Perron operator of diffusion and reaction for the Poincaré–Birkhoff mapping of the system. We show that the rates of exponential relaxation are given by the Pollicott–Ruelle resonances of the Frobenius–Perron operator. We identify the reaction rate among these resonances and we describe its properties. One of our purposes is to understand the conditions under which the reaction is controlled by the chaotic diffusion and to characterize this regime in the special two-dimensional case. Another of our purposes is the construction of the reactive eigenmodes which govern the exponential relaxation of the color. Such eigenmodes have already been constructed for the chaotic diffusion in the multibaker map and in the Lorentz gas, where they are given by singular distributions devoided of a density function.[14, 24, 25] In the reactive Lorentz gas, we obtain a similar result for the

reactive eigenmodes in spite of the fact that the reactive process is a priori random by the introduction of the probability p_0. Such an assumed randomness is often believed to smoothen sufficiently the eigenmodes to guarantee the existence of their density function. Here, we show that such a smoothing does not occur because the randomness is only assumed at some internal boundaries of the system and because the dynamics remains deterministic and chaotic between these boundaries.

Finally, we would like to show that the dynamics of the whole gas containing infinitely many particles is essentially ruled by the chaotic one-particle dynamics in systems such as the one we describe here. In these chaotic one-particle systems, the macroscopic reaction-diffusion equations ruling the relaxation toward the thermodynamic equilibrium can be justified in both the diffusive and reactive sectors of the dynamics.

The plan of the paper is as follows. Section 2 contains a detailed description of the model used. The Frobenius–Perron operator which rules the time evolution of the probability distribution in phase space is derived in Section 3. Its reactive eigenmodes are constructed in Section 4. The large-scale properties of reaction are studied in Section 5 with a random-walk model of the diffusion-reaction process. Conclusions and perspectives are drawn in Section 6.

2. DESCRIPTION OF THE MODEL

In the reactive periodic Lorentz gas, a point particle, carrying a color A or B, undergoes elastic collisions on disks fixed in the plane and forming a regular triangular lattice, characterized by the fundamental lattice vectors $\mathbf{e}_1 = d(1, 0)$ and $\mathbf{e}_2 = d(\frac{1}{2}, \sqrt{3}/2)$. The radius of the disks is assumed equal to unity and d is the distance between the centers of the disks. We shall work in the finite horizon regime, $2 < d < 4/\sqrt{3}$, for which the diffusion coefficient is finite.[19, 20] Some of the disks are catalysts: if the point particle collides on one of them, it changes instantaneously its color with a probability p_0. The catalysts form a regular triangular superlattice over the disk lattice. The fundamental vectors characterizing this superlattice are $\mathbf{E}_1 = nd(0, -\sqrt{3})$ and $\mathbf{E}_2 = nd(\frac{3}{2}, \sqrt{3}/2)$, where n is an integer parameter which controls the density of catalysts in the system: in the directions of $\mathbf{E}_1$ and $\mathbf{E}_2$, one disk over n is a catalyst. The configurations with $n = 1$ and $n = 2$ are depicted in Fig. 1. For $n = 1$, the fundamental cell of the superlattice contains 3 disks among which one is a catalyst and it can be chosen as shown in Fig. 1a. The shape of the fundamental cell for $n = 1$ is used as the building block for the fundamental cell for larger n, as shown in Fig. 1b for the case $n = 2$. Therefore, for larger n, the fundamental cell of the superlattice

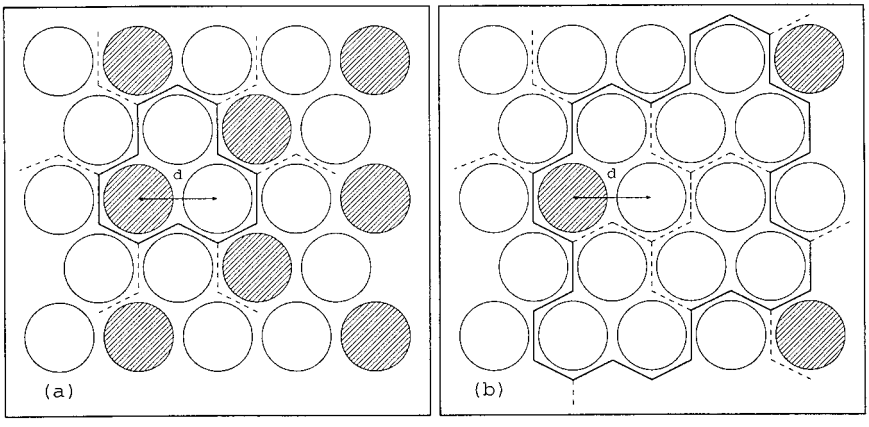

Fig. 1. (a) Elementary cell of the superlattice of the catalysts, in the case $n=1$; (b) in the case $n=2$.

is made of $n \times n$ of these blocks of 3 disks. Accordingly, one disk over $N=3n^2$ is a catalyst. This geometry has been chosen in order to study different densities of catalysts by the same numerical algorithm, which depends on the parameter n. The isomerization is assumed to be isothermal in the sense that the reaction is independent of the energy of the particle. For this reason, the color dynamics is passively driven by the motion of the point particle which, itself, is not affected by the isomerization.

The phase-space coordinates of the point particle are its positions, its velocities and its color (x, y, v_x, v_y, c). The color is labeled by a discrete variable c which takes the values $+1$ or -1 whenever the color is A or B. Since the collisions are elastic, the energy is conserved and the magnitude of the velocity is a constant of motion. We shall restrict ourselves, without loss of generality, to $\|\mathbf{v}\|=1$. This energy shell defines a three-dimensional phase space having the coordinates (x, y, φ, c), where φ is the angle between the velocity and the x-axis.

By the spatial periodicity of the system studied, the dynamics can be reduced to the dynamics inside an elementary cell of the superlattice of catalysts, which contains $N=3n^2$ disks. Moreover, the three-dimensional flow dynamics can be further reduced to a Poincaré–Birkhoff map describing the dynamics from collision to collision. The Birkhoff coordinates are $\mathbf{x}=(j, \theta, \varpi)$ with $1 \leqslant j \leqslant N=3n^2$, $0 \leqslant \theta < 2\pi$ and $-1 \leqslant \varpi \leqslant 1$. j defines the disk of the elementary cell on which the collision takes place, θ is an angle giving the position of the impact on this disk and ϖ is the sine of the angle between the velocity after collision and the normal at the impact.[14, 16, 24]

In these Birkhoff coordinates, the mapping is known to be area-preserving. The mapping of the reactive Lorentz gas is thus given by:

$$\begin{aligned} \mathbf{x}_{n+1} &= \varphi(\mathbf{x}_n) \\ t_{n+1} &= t_n + T(\mathbf{x}_n) \\ \boldsymbol{l}_{n+1} &= \boldsymbol{l}_n + \mathbf{a}(\mathbf{x}_n) \\ c_{n+1} &= \varepsilon(\mathbf{x}_n)\, c_n \end{aligned} \tag{2}$$

t_n is the time of the nth collision. $T(\mathbf{x})$ is the first-return time function. The vector $\boldsymbol{l}_n$ gives the cell of the superlattice visited at time t_n and $\mathbf{a}(\mathbf{x}_n)$ is a vector giving the jump carried out on the superlattice during the free flight from $\mathbf{x}_n$ to $\mathbf{x}_{n+1}$. The change of color is controlled by the function:

$$\varepsilon(\mathbf{x}_n) = \begin{cases} -1 & \text{if } \; j_n \text{ is a catalyst, with a probability } p_0 \\ +1 & \text{otherwise} \end{cases} \tag{3}$$

3. THE FROBENIUS–PERRON OPERATOR: FROM THE FLOW TO THE POINCARÉ–BIRKHOFF MAP

The current state and position of the particle are given by a suspended flow in terms of the coordinates $(\mathbf{x}, \tau, \boldsymbol{l}, c)$, where $0 \leqslant \tau < T(\mathbf{x})$ is the time elapsed since the last collision, $\boldsymbol{l}$ is a vector of the superlattice and $c = \pm 1$. The flow is given by

$$\Phi^t(\mathbf{x}, \tau, \boldsymbol{l}, c) = (\mathbf{x}, \tau + t, \boldsymbol{l}, c), \qquad \text{for} \quad 0 \leqslant \tau + t < T(\mathbf{x}) \tag{4}$$

$$\begin{aligned} \Phi^t(\mathbf{x}, \tau, \boldsymbol{l}, c) = [\, &\varphi^m \mathbf{x},\ \tau + t - T(\mathbf{x}) - \cdots - T(\varphi^{m-1}\mathbf{x}), \\ &\boldsymbol{l} + \mathbf{a}(\mathbf{x}) + \cdots + \mathbf{a}(\varphi^{m-1}\mathbf{x}),\ \varepsilon(\mathbf{x})\, \varepsilon(\varphi\mathbf{x}) \cdots \varepsilon(\varphi^{m-1}\mathbf{x})\, c\,], \\ &\text{for} \quad 0 \leqslant \tau + t - T(\mathbf{x}) - \cdots - T(\varphi^{m-1}\mathbf{x}) < T(\varphi^m \mathbf{x}) \end{aligned} \tag{5}$$

The phase-space probability density $q(\mathbf{x}, \tau, \boldsymbol{l}, c)$ evolves in time under a Frobenius–Perron operator $\hat{P}^t$:

$$(\hat{P}^t q)(\mathbf{x}, \tau, \boldsymbol{l}, c) = q[\, \Phi^{-t}(\mathbf{x}, \tau, \boldsymbol{l}, c)\,] \tag{6}$$

The dynamics of this infinite system can be described by a density defined in an elementary cell of the superlattice and by a Frobenius–Perron operator acting on this density. A detailed derivation of this operator for

the diffusive case is given elsewhere.[14, 24] Only the main steps of the calculation are presented here in the case of our model.

We define a projection operator

$$\hat{E}_{\mathbf{k}} = \sum_{\boldsymbol{l} \in \mathscr{L}} \exp(-i\mathbf{k}\cdot\boldsymbol{l})\, \hat{S}^{\boldsymbol{l}} \tag{7}$$

where $\mathscr{L}$ is the superlattice vectors set and

$$\hat{S}^{\boldsymbol{l}} f(\mathbf{x}, \boldsymbol{l}') = f(\mathbf{x}, \boldsymbol{l}' + \boldsymbol{l}), \qquad \text{with} \quad \boldsymbol{l}, \boldsymbol{l}' \in \mathscr{L} \tag{8}$$

Applying $\hat{E}_{\mathbf{k}}$ to the density $q(\mathbf{x}, \tau, \boldsymbol{l}, c)$ gives

$$\begin{aligned} \hat{E}_{\mathbf{k}} q(\mathbf{x}, \tau, \boldsymbol{l}, c) &= \exp(i\mathbf{k}\cdot\boldsymbol{l})\, \hat{E}_{\mathbf{k}} q(\mathbf{x}, \tau, 0, c) \\ &= \exp(i\mathbf{k}\cdot\boldsymbol{l})\, q_{\mathbf{k}}(\mathbf{x}, \tau, c) \end{aligned} \tag{9}$$

The evolution in time of the density turns out to be decoupled into the different Fourier components $q_{\mathbf{k}}$, which are governed by evolution operators defined as

$$\begin{aligned} \hat{Q}^t_{\mathbf{k}}(\mathbf{x}, \tau, c) &\equiv \hat{E}_{\mathbf{k}} \hat{P}^t q(\mathbf{x}, \tau, 0, c) \\ &= \exp\{ i\mathbf{k}\cdot\boldsymbol{l}[\Phi^{-t}(\mathbf{x}, \tau, 0, c)] \}\; q_{\mathbf{k}}[\phi^{-t}(\mathbf{x}, \tau, c)] \end{aligned} \tag{10}$$

where ϕ^t is the flow in the fundamental cell of the lattice.

In order to reduce the flow dynamics to the mapping from collision to collision, a Laplace transform of $\hat{Q}^t_{\mathbf{k}} q_{\mathbf{k}}(\mathbf{x}, \tau, c)$ is performed:

$$\begin{aligned} &\int_0^\infty dt \exp(-st)\, \hat{Q}^t_{\mathbf{k}}\, q_{\mathbf{k}}(\mathbf{x}, \tau, c) \\ &\quad = \exp(-s\tau) \left[\int_0^\tau d\tau' \exp(s\tau')\, q_{\mathbf{k}}(\mathbf{x}, \tau', c) + \sum_{n=1}^{\infty} \hat{R}^n_{\mathbf{k}, s} \tilde{q}_{\mathbf{k}, s}(\mathbf{x}, c) \right] \end{aligned} \tag{11}$$

where $\tilde{q}_{\mathbf{k}, s}$ is a function defined by

$$\tilde{q}_{\mathbf{k}, s}(\mathbf{x}, c) = \int_0^{T(\mathbf{x})} d\tau' \exp(s\tau')\, q_{\mathbf{k}}(\mathbf{x}, \tau', c) \tag{12}$$

$\hat{R}_{\mathbf{k}, s}$ is the Frobenius–Perron operator of the mapping φ describing the evolution from collision to collision, and multiplied by an important factor which takes into account the varying time of flight between the collisions,

the spatial modulation by the wavenumber $\mathbf{k}$, as well as the color change on a part of the domain of definition of the Poincaré–Birkhoff mapping:

$$\hat{R}_{\mathbf{k},s}\tilde{q}_{\mathbf{k},s}(\mathbf{x},c) = \exp[-sT(\varphi^{-1}\mathbf{x}) - i\mathbf{k}\cdot\mathbf{a}(\varphi^{-1}\mathbf{x})] \times \{[1-p(\varphi^{-1}\mathbf{x})]\,\tilde{q}_{\mathbf{k},s}(\varphi^{-1}\mathbf{x},c) + p(\varphi^{-1}\mathbf{x})\,\tilde{q}_{\mathbf{k},s}(\varphi^{-1}\mathbf{x},-c)\} \tag{13}$$

where

$$p(\mathbf{x}=\{j,\theta,\varpi\}) = \begin{cases} p_0 & \text{if } j \text{ is a catalyst} \\ 0 & \text{otherwise} \end{cases} \tag{14}$$

We define the total phase-space density $f(\mathbf{x})$ and the difference $g(\mathbf{x})$ of phase-space densities as

$$f(\mathbf{x}) = \tilde{q}(\mathbf{x},A) + \tilde{q}(\mathbf{x},B) \tag{15}$$

$$g(\mathbf{x}) = \tilde{q}(\mathbf{x},A) - \tilde{q}(\mathbf{x},B) \tag{16}$$

The density $f(\mathbf{x})$ does not distinguish the colors and evolves as in the nonreactive Lorentz gas.[14, 24] The difference $g(\mathbf{x})$ of color densities is expected to relax to zero, describing the relaxation toward equilibrium. The time evolutions of these two quantities are decoupled and governed by the following operators:

$$\hat{V}_{\mathbf{k},s}f(\mathbf{x}) = \exp[-sT(\varphi^{-1}\mathbf{x}) - i\mathbf{k}\cdot\mathbf{a}(\varphi^{-1}\mathbf{x})]\,f(\varphi^{-1}\mathbf{x}) \tag{17}$$

and

$$\hat{W}_{\mathbf{k},s}g(\mathbf{x}) = [1-2p(\varphi^{-1}\mathbf{x})]\exp[-sT(\varphi^{-1}\mathbf{x}) - i\mathbf{k}\cdot\mathbf{a}(\varphi^{-1}\mathbf{x})]\,g(\varphi^{-1}\mathbf{x}) \tag{18}$$

The operator $\hat{V}_{\mathbf{k},s}$ controls the diffusive motion of the total density $f(\mathbf{x})$ and has been studied elsewhere.[14, 24] The operator $\hat{W}_{\mathbf{k},s}$ governs the evolution of the difference of densities between both colors $g(\mathbf{x})$ and is thus associated with the reaction. These operators are composed of the Frobenius–Perron operator of the Poincaré–Birkhoff mapping and of an operator of multiplication by a complex function of the coordinates.

The relaxation toward equilibrium can be studied by the spectral analysis of these operators. In particular, an exponential decay at the rate $-s$ can be identified by considering the eigenvalue problems based on these operators. Assuming an eigenvalue equal to unity for these operators has the effect of fixing the decay rate $-s$ to be a function of the wavenumber $\mathbf{k}$.

The so-obtained decay rate $-s_{\mathbf{k}}$ is a so-called Pollicott–Ruelle resonance[17, 18] and it would correspond to a sort of eigenvalue for the Liouvillian operator of the system.[14] Since this rate is a function of the wavenumber it gives a dispersion relation for the process. We notice that the operator (17) reduces to the Frobenius–Perron operator for the Poincaré–Birkhoff map of the billiard composed of a single cell of the periodic Lorentz gas if the wavenumber vanishes. We know that this billiard is ergodic and possesses a unique invariant measure which has a uniform density,[19, 20] so that we may conclude that the resolution of the eigenvalue problem for the operator (17) would give $s_0 = 0$ for the leading solution s. If the wavenumber is now increased from zero, a branch of solutions $s_{\mathbf{k}}$ is obtained which starts from $s_0 = 0$. This branch defines the dispersion relation of diffusion and the corresponding eigenmode defines the hydrodynamic mode of diffusion in the Lorentz gas, as studied elsewhere.[14, 24]

4. REACTIVE EIGENMODES OF THE REACTIVE PERIODIC LORENTZ GAS

4.1. Relaxation Rates

The reaction can be studied in a similar way as the diffusion by identifying the eigenmode of the operator (18) which controls the slowest relaxation of the color. Accordingly, we consider the Pollicott–Ruelle resonances of the reactive operator (18) since these resonances provide the relaxation rates of the reactive eigenmodes. To obtain these resonances, we consider the generalized eigenvalue problem for $\hat{W}_{\mathbf{k},s_{\mathbf{k}}}$, and its adjoint $\hat{W}^{\dagger}_{\mathbf{k},s_{\mathbf{k}}}$ with 1 as eigenvalue[14, 24]

$$\hat{W}_{\mathbf{k},s_{\mathbf{k}}}\psi_{\mathbf{k}}(\mathbf{x}) = \psi_{\mathbf{k}}(\mathbf{x}) \tag{19}$$

$$\hat{W}^{\dagger}_{\mathbf{k},s_{\mathbf{k}}}\tilde{\psi}_{\mathbf{k}}(\mathbf{x}) = \tilde{\psi}_{\mathbf{k}}(\mathbf{x}) \tag{20}$$

assuming the normalization condition

$$\langle \tilde{\psi}_{\mathbf{k}}\psi_{\mathbf{k}} \rangle = 1 \tag{21}$$

A formal solution for $\psi_{\mathbf{k}}$ (respectively $\tilde{\psi}_{\mathbf{k}}$) can be obtained by applying successively $\hat{W}_{\mathbf{k},s}$ (respectively $\hat{W}^{\dagger}_{\mathbf{k},s}$) to the unit function:

$$\psi_{\mathbf{k}}(\mathbf{x}) = \lim_{n\to\infty} \prod_{m=1}^{n} [1 - 2p(\varphi^{-m}\mathbf{x})] \exp[-s_{\mathbf{k}} T(\varphi^{-m}\mathbf{x}) - i\mathbf{k}\cdot\mathbf{a}(\varphi^{-m}\mathbf{x})] \tag{22}$$

$$\tilde{\psi}_{\mathbf{k}}(\mathbf{x}) = \lim_{n\to\infty} \prod_{m=0}^{n-1} [1 - 2p(\varphi^{m}\mathbf{x})] \exp[-s_{\mathbf{k}} T(\varphi^{m}\mathbf{x}) - i\mathbf{k}\cdot\mathbf{a}(\varphi^{m}\mathbf{x})] \tag{23}$$

The normalization condition gives an equation to obtain $s_{\mathbf{k}}$:

$$1 = \lim_{n \to \infty} \left\langle \prod_{m=-n}^{n-1} [1 - 2p(\varphi^m \mathbf{x})] \exp[-s_{\mathbf{k}} T(\varphi^m \mathbf{x}) - i\mathbf{k} \cdot \mathbf{a}(\varphi^m \mathbf{x})] \right\rangle \quad (24)$$

We are interested in the smallest relaxation rate $-s_{\mathbf{k}}$ which dominates at long times t. For the reactive case, the dispersion relation is given by

$$s_{\mathbf{k}} = -2\kappa - D^{(r)}\mathbf{k}^2 + \mathcal{O}(\mathbf{k}^4) \quad (25)$$

where κ is the reaction rate which is thus given by

$$\kappa = -\tfrac{1}{2} s_0 \quad (26)$$

This method can be efficiently applied to the numerical computation of the reaction rate. An example of dispersion relation for the reaction is depicted in Fig. 2 where we see that the quadratic approximation holds up to the wavenumber ($k_x = 0.08$, $k_y = 0$) in this case where $d = 2.1$, $n = 2$, and $p_0 = 0.1$. In this example, the reaction rate takes the value $\kappa = 0.0095$, while the reactive diffusion coefficient has the value $D^{(r)} = 0.091 \pm 0.007$ which is very close to the value of the diffusion coefficient $D = 0.0995 \pm 0.0003$.[23]

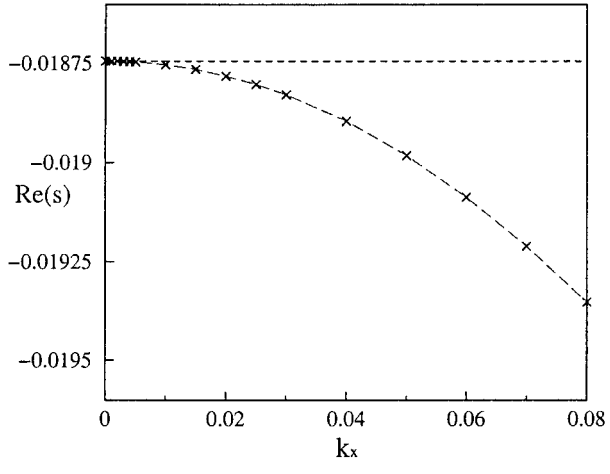

Fig. 2. Dispersion relation in the reactive case, as function of k_x, $k_y = 0$, for $d = 2.1$, $n = 2$, $p_0 = 0.1$; $2\kappa = 0.01875$ and $D^{(r)} = 0.091$. The imaginary part $Im(s)$ is equal to zero within the numerical error.

4.2. Cumulative Functions of the Reactive Eigenmodes

The cumulative function of the reactive eigenmode is obtained by integration of (22) over θ and ϖ. For a vanishing wavenumber $\mathbf{k}=0$, we get

$$F_0(j,\theta,\varpi)=\frac{1}{4\pi}\int_0^{\theta}d\theta'\int_{-1}^{\varpi}d\varpi'\lim_{n\to\infty}\times\prod_{m=1}^{n}[1-2p(\varphi^{-m}\mathbf{x}')]\exp[+2\kappa T(\varphi^{-m}\mathbf{x}')] \qquad (27)$$

For the reactive Lorentz gas with $n=2$ and $d=2.1$, this cumulative function is depicted in Fig. 3a on the phase-space region of the catalyst and in Fig. 3b on the region of the nearest-neighboring disk at the right-hand side of the catalyst.

The contribution of an initial condition (θ,ϖ) to the integral (27) depends on the number n' of collisions on a catalyst during the trajectory. The larger n' is, the smaller the contribution of the trajectory from the initial condition (θ,ϖ). The global slope of $F_0(j,\theta,\varpi)$ is thus smaller for values of (θ,ϖ) giving trajectories with many collisions on catalysts. This effect becomes more and more pronounced as p_0 increases. This can be seen in Figs. 3a and 3b. Figure 3a depicts the cumulative function around

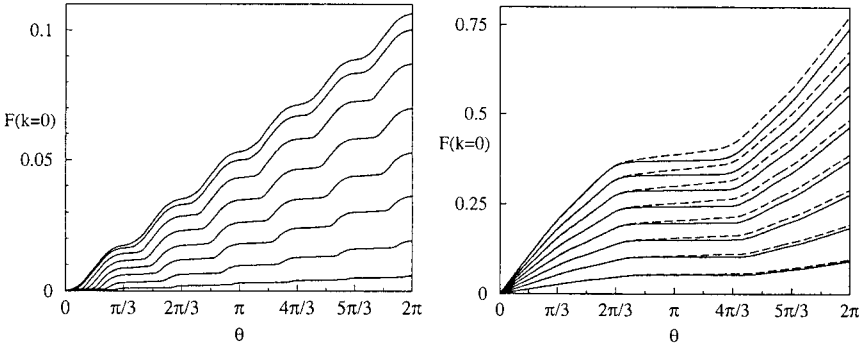

Fig. 3. (a) Cumulative function of the eigenstates around the catalyst at vanishing wavenumber $\mathbf{k}=0$, for $d=2.1$, $n=2$, $p_0=0.4$; $\varpi=-0.75,\ -0.5,\ -0.25,\ 0,\ 0.25,\ 0.5,\ 0.75,\ 1$; (b) Cumulative function of the eigenstates around a disk first neighbor of the catalyst at vanishing wavenumber $\mathbf{k}=0$, for $d=2.1$, $n=2$, $p_0=0.2$ for the dashed line, $p_0=0.4$ for the solid line, $\varpi=-0.75,\ -0.5,\ -0.25,\ 0,\ 0.25,\ 0.5,\ 0.75,\ 1$. In both figures, the functions are given up to a multiplicative constant.

a catalytic disk. The sixfold structure is due to the six openings toward the next-nearest-neighboring disks. However, Fig. 3b depicts the cumulative function on a disk which is on the right-hand side of the catalytic disk so that reaction occurs for the angle θ around the value π and, indeed, the slope of the cumulative function is smaller in this region than for other angles where the nearest-neighboring disk is not catalytic.

The cumulative functions of the eigenstates are continuous but are not differentiable like Lebesgue's singular functions.[26, 27] One of such singular functions is plotted in the book by Billingsley in the one-dimensional case.[26] Here, we have a function defined in the two-dimensional phase space of Birkhoff coordinates. At each point, one direction is unstable and another is stable although these directions do not vary continuously as it is known for the map of the Lorentz-gas billiard.[19, 20] Because the unstable direction is expanding, the density is smooth in this direction so that the singular character is only expected in the stable direction.[24, 25] Since the cumulative function (27) involves the inverse of the mapping φ^{-1}, an expanding dynamics is expected to occur in the stable direction along which the cumulative function (27) is singular.

In order to understand better what happens in the stable direction, we consider an analogy with an expanding one-dimensional r-adic map:[26, 27]

$$x_{n+1} = r x_n, \qquad \text{(modulo 1)} \tag{28}$$

Each initial condition of a trajectory of the map (28) corresponds to a symbolic sequence $\{\omega_n\}_{n=0}^{\infty}$ according to

$$x = \sum_{n=1}^{\infty} \frac{\omega_{n-1}}{r^n} \tag{29}$$

with $\omega_n = 0, 1, 2, \ldots, r-1$. Each symbolic sequence of n symbols corresponds to an interval of length $1/r^n$ on the unit interval where the one-dimensional map (28) is defined. For such a map, the first-return time is $T = 1$ so that the density of the reactive eigenmode (22) with $\mathbf{k} = 0$ has the form

$$\psi(x) = \lim_{n \to \infty} u_{\omega_0} u_{\omega_1} u_{\omega_2} \cdots u_{\omega_{n-1}} \exp(-sn) \tag{30}$$

where $u_\omega = 1$ if the subinterval ω is non-reactive and $u_\omega = 1 - 2p_0$ if it is reactive, for instance. Requiring that the density (30) is normalized by $\int_0^1 \psi(x)\, dx = 1$ leads to the value of the decay rate $s = \ln(\sum_\omega u_\omega / r)$. If we introduce $v_\omega = u_\omega \exp(-s) = r u_\omega / \sum_\omega u_\omega$, which satisfy $\sum_\omega v_\omega = r$, the density (30) can be rewritten as

$$\psi(x) = \lim_{n \to \infty} v_{\omega_0} v_{\omega_1} v_{\omega_2} \cdots v_{\omega_{n-1}} = \lim_{n \to \infty} \left(\prod_{\omega=0}^{r-1} v_\omega^{f_\omega(x,n)} \right)^n \tag{31}$$

where $f_\omega(x, n)$ is the frequency of occurrence of the symbol ω among the n first symbols of the r-adic expansion (29) of x. All the frequencies add up to unity: $\sum_\omega f_\omega(x, n) = 1$. It is known that the invariant measure of the r-adic map (28) has a uniform density so that these frequencies are all equal to $1/r$ for almost all the initial conditions x of the unit interval. For this reason, the cumulative function

$$F(x) = \int_0^x \psi(x')\, dx' \tag{32}$$

is a Lebesgue singular functions unless $u_\omega = 1$ for all $\omega = 0, 1, 2, ..., r-1$, in which case $F(x) = x$. The cumulative function for the r-adic map is the solution of the deRham-type iteration[27, 28]

$$F(x) = \exp(-s) \times \begin{cases} \dfrac{u_0}{r} F(rx), & 0 < x < \dfrac{1}{r} \\ \dfrac{u_1}{r} F(rx-1) + \dfrac{u_0}{r} F(1), & \dfrac{1}{r} < x < \dfrac{2}{r} \\ \dfrac{u_2}{r} F(rx-2) + \dfrac{u_0+u_1}{r} F(1), & \dfrac{2}{r} < x < \dfrac{3}{r} \\ \vdots & \\ \dfrac{u_{r-1}}{r} F(rx-r+1) + \dfrac{u_0+u_1+\cdots+u_{r-2}}{r} F(1), & \dfrac{r-1}{r} < x < 1 \end{cases} \tag{33}$$

Figure 4 shows two examples of this cumulative function in the triadic case $r = 3$, $u_0 = u_2 = 1$ and $u_1 = 1 - 2p_0$ for $p_0 = 0.2$ and $p_0 = 0.4$. The eigenvalue is here $\exp(s) = 1 - 2p_0/3$. We observe that the singular character increases with p_0 although the function can be innocent looking for small values of p_0. We also observe that the slope of the cumulative function decreases in a reactive region as p_0 increases in the same way as in Fig. 3b for the reactive Lorentz gas.

In general, the cumulative function (32) is continuous and increasing but its derivative is zero almost everywhere, i.e., where $\psi(x) = 0$. Furthermore, its derivative is infinite on a dense set of points where $\psi(x) = +\infty$. To show these properties and the analogy with the general cumulative

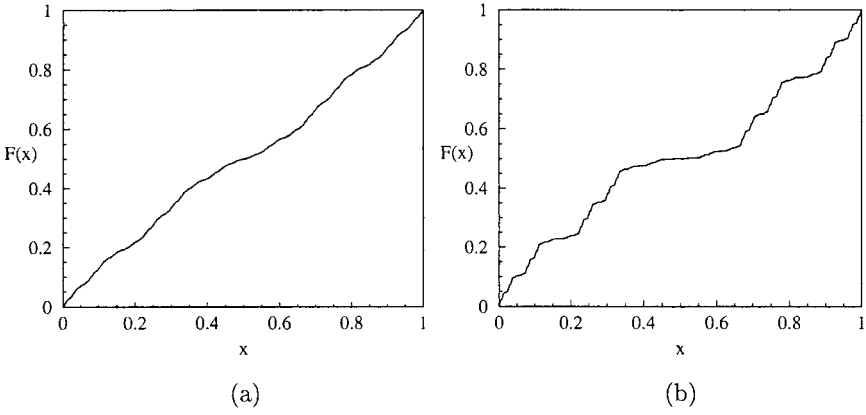

Fig. 4. (a) Cumulative function of the eigenstates of the reactive r-adic map (28) for $r=3$, $u_0=1$, $u_1=1-2p_0$, $u_2=1$ with: (a) $p_0=0.2$; (b) $p_0=0.4$. The cumulative function is here numerically calculated by iterating the deRham-type system (33).

function (27), let us consider the dyadic case with $r=2$. In this dyadic case, we find that

$$\begin{cases} \psi(x)=0, & \text{if} \quad v_0^{f_0(x,n)} v_1^{f_1(x,n)} < 1 \\ \psi(x)=+\infty, & \text{if} \quad v_0^{f_0(x,n)} v_1^{f_1(x,n)} > 1 \end{cases} \tag{34}$$

for $n \to \infty$, where $v_0+v_1=2$ and $f_0+f_1=1$. Moreover, we know that $f_0=f_1=1/2$ for the binary expansion, of almost all the points x of the unit interval, so that the density takes the value $\psi(x)=\lim_{n\to\infty}(v_0 v_1)^{n/2}$ for almost all the points x. Since $v_0+v_1=2$, we get that

$$v_0 v_1 = 1-(v_0-1)^2 < 1 \tag{35}$$

unless $v_0=v_1=1$. Therefore, $\psi(x)=0$ for almost all the points x, which means that its cumulative function $F(x)$ has a zero derivative almost everywhere. However, the derivative of $F(x)$ is infinite where $\psi(x)$ is infinite, which occurs if

$$f_0(x,n) > f_c = \frac{\ln(1/v_1)}{\ln(v_0/v_1)} > \frac{1}{2} \tag{36}$$

for $n \to \infty$. Because the critical frequency f_c is larger than $1/2$ if $v_0 \neq 1$, we infer that $\psi(x)$ is infinite only on a set of zero Lebesgue measure but this set is dense in the unit interval. For instance, the points x such that $f_0=1$ and $f_1=0$ are dense. Indeed, this set contains the points x with a binary expansion like $\omega_0\omega_2\omega_2\cdots\omega_{n-1}00000000\cdots$ with n arbitrarily large. These

points delimit the intervals of length $\Delta x = 1/2^n$ obtained by dividing the unit interval successively n times into two equal pieces. For $n \to \infty$, these points are dense in the unit interval so that we may conclude that $\psi(x) = +\infty$ on a set which is dense in $0 \leqslant x \leqslant 1$.

The cumulative function (27) of the reactive Lorentz gas differs from the one of piecewise-linear maps in several respects. Firstly, the mapping φ of the disk billiard is nonlinear and the stable direction changes from point to point. Therefore, the singular character is here expected to occur along the changing stable direction.[14, 24] Secondly, the first-return time function is not constant in a billiard but we should notice here the decay rate $-s$ appearing in the cumulative function (27) is fixed by the normalization condition (24) so that the cumulative function (27) exists only for that value of the decay rate $-s$. Despite these differences, the same behavior happens for the density of the cumulative function (27) as for the Lebesgue singular function. Indeed, this density can be rewritten as

$$\psi_0(\mathbf{x}) = \lim_{n \to \infty} [(1 - 2p_0)^{f_{\text{catalyst}}(\mathbf{x}, n)} \mathrm{e}^{+2\kappa \mathscr{T}(\mathbf{x}, n)}]^n \tag{37}$$

where $f_{\text{catalyst}}(\mathbf{x}, n)$ is the frequency of collision on a catalyst and $\mathscr{T}(\mathbf{x}, n)$ is the mean intercollisional time, during the n first collisions of the trajectory from the initial condition $\mathbf{x} = (j, \theta, \varpi)$. We notice that this density is non-negative for a reaction probability $0 \leqslant p_0 < 1/2$. If $\mathbf{x}$ is the initial condition of a trajectory without collision on any catalyst after the $\mathscr{N}$th collision, all the factors corresponding to the further collisions are larger than one so that $\psi_0(\mathbf{x}) = +\infty$ for such trajectories. These trajectories are dense because they can be as close as possible to an arbitrary trajectory for a large enough value of $\mathscr{N}$ since the system is dynamically unstable and ergodic. On the other hand, the density vanishes for almost all the other trajectories if the reaction probability p_0 is positive and small enough. We may therefore conclude that the cumulative function (27) of the reactive eigenmode of the reactive Lorentz gas is a kind of two-dimensional generalization of Lebesgue's singular functions.

5. THE REACTION RATE

5.1. The Macroscopic Reaction-Diffusion Equations

In order to derive an equation for the macroscopic difference of color densities

$$\sigma(\boldsymbol{l}, t) = \rho_A(\boldsymbol{l}, t) - \rho_B(\boldsymbol{l}, t) \tag{38}$$

we go back to the eigenvalue problem for the flow. It is given by

$$\hat{Q}^t_{\mathbf{k}} \Psi_{\mathbf{k}}(\mathbf{x}, \tau) = \exp(s_{\mathbf{k}} t)\ \Psi_{\mathbf{k}}(\mathbf{x}, \tau) \tag{39}$$

where $\Psi_{\mathbf{k}}(\mathbf{x}, \tau)$ is related to the eigenstate of the mapping $\psi_{\mathbf{k}}(\mathbf{x})$ by[14, 24]

$$\Psi_{\mathbf{k}}(\mathbf{x}, \tau) = \exp(-s_{\mathbf{k}} \tau)\ \psi_{\mathbf{k}}(\mathbf{x}) \tag{40}$$

Equation (39) can be rewritten as

$$\hat{E}_{\mathbf{k}} \hat{P}^t \Psi(\mathbf{x}, \tau, 0) = \exp(s_{\mathbf{k}} t)\ \Psi_{\mathbf{k}}(\mathbf{x}, \tau) \tag{41}$$

and can be generalized to any vector $\boldsymbol{l} \in \mathscr{L}$ by

$$\hat{E}_{\mathbf{k}} \hat{P}^t \Psi(\mathbf{x}, \tau, \boldsymbol{l}) = \exp(i\mathbf{k} \cdot \boldsymbol{l}) \exp(s_{\mathbf{k}} t)\ \Psi_{\mathbf{k}}(\mathbf{x}, \tau) \tag{42}$$

The macroscopic difference of concentrations is obtained by integration of (42) over $\mathbf{x} = (j, \theta, \varpi)$ and over τ:

$$\sigma(\boldsymbol{l}, t) = \exp(i\mathbf{k} \cdot \boldsymbol{l}) \exp(s_{\mathbf{k}} t) \frac{1}{3n^2} \sum_{j=1}^{3n^2} \frac{1}{4\pi} \int_0^{2\pi} d\theta \int_{-1}^{1} d\varpi \frac{1}{\langle T \rangle}$$
$$\times \int_0^{T(\mathbf{x})} d\tau\ \Psi_{\mathbf{k}}[\mathbf{x} = (j, \theta, \varpi), \tau] \tag{43}$$

where $\langle T \rangle$ is the mean value of $T(\mathbf{x})$. The temporal evolution of $\sigma(\boldsymbol{l}, t)$ at long time t will be dominated by the leading dispersion relation $s_{\mathbf{k}}$ given by (25). On large spatial scales, the behavior is ruled by the dispersion relation expanded up to the terms which are quadratic in the wavenumber. Under these circumstances, we may infer that the difference σ of color densities satisfies the equation

$$\frac{\partial \sigma}{\partial t} \simeq D^{(r)} \frac{\partial^2 \sigma}{\partial \boldsymbol{l}^2} - 2\kappa\sigma \tag{44}$$

approximated to the second-order spatial derivatives. The study of the diffusive case made in refs. 14 and 24, leads to the following macroscopic equation for the total concentration $\rho(\boldsymbol{l}, t) = \rho_A(\boldsymbol{l}, t) + \rho_B(\boldsymbol{l}, t)$

$$\frac{\partial \rho}{\partial t} \simeq D \frac{\partial^2 \rho}{\partial \boldsymbol{l}^2} \tag{45}$$

The combination of Eqs. (44) and (45) corresponds to the macroscopic reaction-diffusion system

$$\frac{\partial \rho_A}{\partial t} \simeq \frac{D+D^{(r)}}{2}\frac{\partial^2 \rho_A}{\partial \boldsymbol{l}^2} + \frac{D-D^{(r)}}{2}\frac{\partial^2 \rho_B}{\partial \boldsymbol{l}^2} - \kappa(\rho_A - \rho_B) \tag{46}$$

$$\frac{\partial \rho_B}{\partial t} \simeq \frac{D-D^{(r)}}{2}\frac{\partial^2 \rho_A}{\partial \boldsymbol{l}^2} + \frac{D+D^{(r)}}{2}\frac{\partial^2 \rho_B}{\partial \boldsymbol{l}^2} + \kappa(\rho_A - \rho_B) \tag{47}$$

We find cross-diffusion terms between both chemical species, which are similar to the ones obtained in the reactive multibaker map.[15] These cross-diffusive terms have their origin in the fact that the equations (46)–(47) hold on spatial scales which are larger than the distance L between the catalysts: $\|\boldsymbol{l}\| \gg L$. On spatial scales which are smaller than the distance between the catalysts but larger than the lattice interdisk distance, we should expect a pure diffusive motion of each species A and B without cross-diffusion.[16] Indeed, the motion between the catalysts is diffusive and the species does not change as long as a catalyst is not met. However, on spatial scales larger than the intercatalyst distance, the chemical species mix so that this cross-diffusion appears. Nevertheless, this cross-diffusion is not expected to be important, for instance, in the case of Fig. 2 where $d = 2.1$, $n = 2$, and $p_0 = 0.1$. In this case, the diffusion coefficient takes the value $D = 0.0995 \pm 0.0003$,[23] although the reactive diffusion coefficient is $D^{(r)} = 0.091 \pm 0.007$. Whereupon the diffusion coefficients are $D_{AA} = D_{BB} = (D + D^{(r)})/2 = 0.095 \pm 0.004$ while the cross-diffusion coefficients are $D_{AB} = D_{AB} = (D - D^{(r)})/2 = 0.004 \pm 0.004$, which is thus a small if not vanishing effect.

5.2. Dependence of the Reaction Rate on the Interdisk Distance

We have calculated numerically the reaction rate by using the normalization condition (24), which allows us to determine the relaxation rate $-s$ as a function of the wavenumber $\mathbf{k}$. The reaction rate is obtained at zero wavenumber by Eq. (26). The dependence of κ on the interdisk distance d has been obtained for three different densities of catalysts, for $n = 1$, 2 and 3 (see Figs. 5a–c). These configurations correspond respectively to one catalyst over 3, 12 and 27 disks.

The reaction rate κ of the first configuration with $n = 1$ is shown in Fig. 5a where we observe that κ decreases as d increases. The values obtained are well fitted by a simple formula: κ is equal to the product of the probability of reaction p_0 with the collision rate and with the fraction

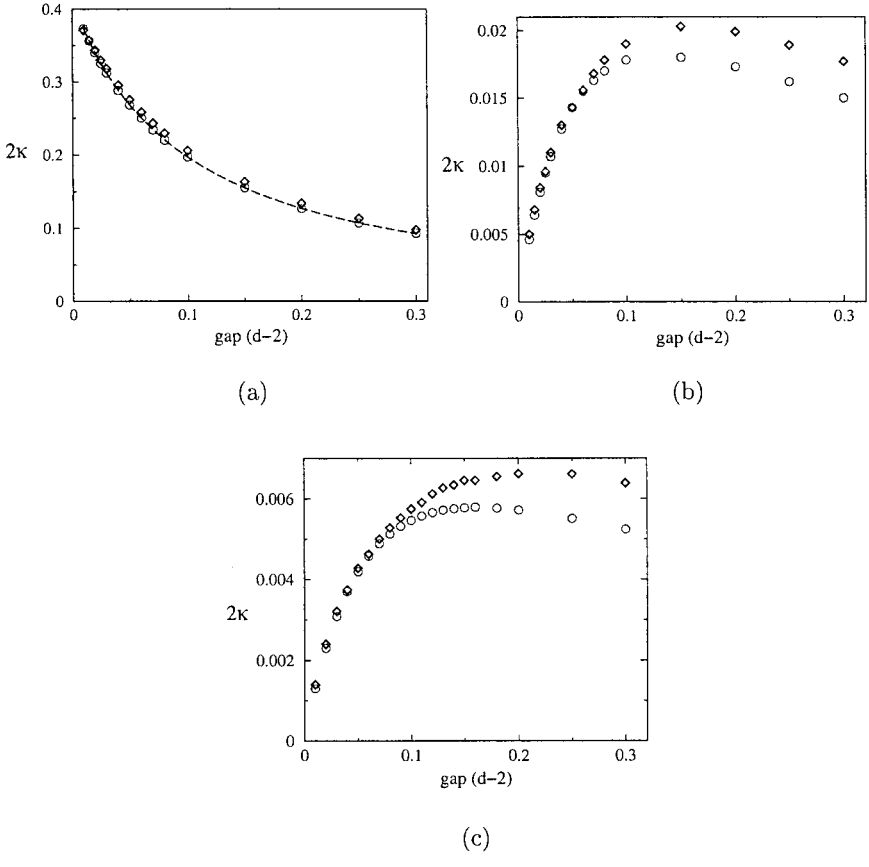

Fig. 5. Reaction rate as a function of d; the diamonds are the resonances of the Frobenius–Perron operator and the circles are the eigenvalues of the transition matrix $\tilde{W}$: (a) for $n=1$, $p_0=0.1$ where the dashed line represents the formula (48); (b) for $n=2$, $p_0=0.1$; (c) for $n=3$, $p_0=0.1$.

of collisions on a catalyst. Since there are three disks in each reactive trap, one of which being the catalyst, the fraction of collisions on the catalyst is 1/3 so that

$$\kappa=\frac{p_0}{3T_{\mathrm{col}}} \tag{48}$$

where

$$T_{\mathrm{col}}=\frac{\sqrt{3}}{4}d^2-\frac{\pi}{2} \tag{49}$$

is the average time between collisions in a trap formed by the region delimited by three nearest-neighboring disks.[29] The reason at the origin of the behavior (48) is that all the traps are reactive in this configuration of the catalysts where $n=1$. Therefore, the reaction is determined simply by the average time between the collisions on the disks and not by the time to jump from one trap to the next.

The reaction rate κ of the other configurations with $n \geqslant 2$ is shown in Fig. 5b and 5c. In these configurations, the density of catalysts is lower and the behavior of κ as a function of the interdisk distance d changes completely. Now, κ vanishes if $d=2$, i.e., if the disks are in contact; κ increases with d, reaches a maximum and then slowly decreases. Here, the particle has to diffuse from trap to trap in order to reach a catalyst before reacting: the reaction is thus controlled by the diffusion for $n \geqslant 2$. This diffusion-reaction process can be modeled by a random-walk approximation similar to the model of Machta and Zwanzig for diffusion.[29] The exact motion of the particle among the disks is replaced by a random walk on the lattice of the traps (see Fig. 6). A trap is reactive if one of the three disks surrounding it is a catalyst. Otherwise, it is non-reactive. This model is assumed to be a Markov process. This will be the case for d near to 2, when the particle undergoes many collisions before leaving a trap. The traps form a regular hexagonal lattice and the reactive traps form a regular hexagonal superlattice over it. By periodicity, we can thus restrict ourselves to an elementary cell.

$f_{i\alpha}$ is defined as the probability to find the particle in the trap i in the state α. $f_{i\alpha}$ is supposed to obey the following master equation:

$$\frac{d}{dt} f_{i\alpha} = \sum_{j\beta} W_{i\alpha j\beta} f_{j\beta} \tag{50}$$

where $W_{i\alpha j\beta}$ is the probability to go from $i\alpha$ to $j\beta$ per unit time. The conservation of probability implies that

$$W_{i\alpha i\alpha} = - \sum_{i\alpha \neq j\beta} W_{i\alpha j\beta} \tag{51}$$

If a particle is in the trap i, it can only stay in it or go to one of the three neighboring traps. Moreover, reaction will be assumed to occur only for a particle being in a reactive trap, without leaving it. Each row i of the

matrix W will have 4 non-zero elements, if i labels a non-reactive trap and 5 otherwise. These non-zero elements can be of 4 different types:

1. Transition from a trap to one of its neighbors: The average residence time in a trap is given by $T_{\rm res} = (\pi/6(d-2))((\sqrt{3}/2)\, d^2 - \pi)$.[29] If we suppose that the three neighbors of a trap are equiprobable, the transition rate is given by $1/3T_{\rm res}$.

2. Reaction in a reactive trap: The reaction rate is supposed equal to $p_0/3T_{\rm col}$.

3. Diagonal element for a reactive trap: According to (51), the diagonal element is equal to $-(p_0/3T_{\rm col}) - (1/T_{\rm res})$.

4. Diagonal element for a non-reactive trap: By the same argument, we have here $-1/T_{\rm res}$.

As a consequence of Eq. (50), the difference of probabilities between both colors $g_i = f_{iA} - f_{iB}$ obeys the equation

$$\frac{d}{dt}(f_{iA} - f_{iB}) = \sum_{j\gamma} (W_{iAj\gamma} - W_{iBj\gamma})\, f_{j\gamma}$$

$$= \sum_{j} [(W_{iAjA} - W_{iBjA})\, f_{jA} + (W_{iAjB} - W_{iBjB})\, f_{jB}] \qquad (52)$$

We notice that the matrix W has the symmetries

$$W_{iAjA} = W_{iBjB} \qquad (53)$$

$$W_{iBjA} = W_{iAjB} \qquad (54)$$

so that Eq. (52) becomes

$$\frac{d}{dt}(f_{iA} - f_{iB}) = \sum_{j} (W_{iAjA} - W_{iBjA})(f_{jA} - f_{jB}) \qquad \text{or} \qquad (55)$$

$$\frac{d}{dt}\, g_i = \sum_{j} \tilde{W}_{ij}\, g_i \qquad (56)$$

An eigenvalue $\lambda^{(\gamma)}$ of the matrix $\tilde{W}$ contributes to the decay of the observable color

$$C(t) = \sum_{i} g_i(t) \qquad (57)$$

only if the autocorrelation function of $C(t)$ is a non-zero function. Since

$$\begin{aligned}\langle C(0)\, C(t)\rangle &= \sum_i g_i^{(\gamma)}(0) \sum_j g_j^{(\gamma)}(t) \\ &= \sum_i g_i^{(\gamma)}(0) \sum_j \exp(\lambda^{(\gamma)} t)\, g_j^{(\gamma)}(0) \\ &= \exp(\lambda^{(\gamma)} t) \left(\sum_i g_i^{(\gamma)} \right)^2 \end{aligned} \tag{58}$$

we obtain the condition that $\sum_i g_i^{(\gamma)}$ must be a non-vanishing quantity. The first eigenvalue satisfying this condition gives the value of the reaction rate as $\kappa = -\lambda^{(\gamma)}/2$. These eigenvalues have been compared with the reaction rates obtained from the reactive evolution operator (18), and with the results of a continuous-time simulation, for $n = 1$, 2 and 3. For $n = 1$, the agreement is good for the whole range of d (see Fig. 5a). The diffusion does not play any role since all traps are reactive. For $n = 2$ and 3, the agreement is good only for the small values of $d - 2$, up to 0.08 (see Fig. 5b–c). This is the range of validity of the random-walk approximation. For larger values of d, we already know that the random-walk model by Machta and Zwanzig does not predict accurate values for the diffusion coefficient since the simple Markov approximation assumed in this model starts to be defective because the flow of particles from one trap to the next traps is more important so that the quasi-equilibrium assumed in each trap is no longer valid.[30] We should therefore expect that the same defect appears here for the reaction rate. A better model for the reaction rate could be obtained with an improved model for the diffusion.

5.3. Dependence of the Reaction Rate on the Intercatalyst Distance

The previous random-walk model has also been used to calculate the reaction rate for more dilute systems with $n = 5$ to 10 for which there is one catalyst over $N = 75$, 108, 147, 192, 243, and 300 disks, respectively. In this dilute regime, the reaction is controlled by the diffusion of the particle between the catalysts so that, in two dimensions, the dependence of κ on N is expected to be

$$\kappa \simeq C \frac{D}{d^2 N \ln N} \tag{59}$$

where D is the diffusion coefficient, d is the interdisk distance, and C is a dimensionless constant. This result is obtained by a calculation based on

Smoluchowski's model.[22] An equation of diffusion is considered for the densities ρ_A and ρ_B and for their difference $\sigma = \rho_A - \rho_B$

$$\partial_t \sigma = D \nabla^2 \sigma \tag{60}$$

where $\nabla = \partial_{\mathbf{r}} = \partial_{\mathbf{l}}$. We notice that this equation only holds for distances which are larger than the interdisk distance but smaller than the intercatalyst distance. In this respect, the cross-diffusive and the reactive terms of Eqs. (46)–(47) do not arise on these intermediate spatial scales.

The diffusion equation (60) must be solved with boundary conditions which suppose that the particles move diffusively toward each catalyst. At the catalyst, we may consider the general radiative boundary condition[3, 22]

$$\partial_r \sigma|_{r=d/2} = \alpha \sigma|_{r=d/2} \tag{61}$$

where the constant α is fixed by the geometry of the catalyst and by the reaction probability p_0. In the present case, since the catalyst does not perturb the geometry of the lattice on which diffusion occurs, we find that $g_i = 0$ on the six traps around a catalyst so that $\alpha = \infty$. However, we shall see that the final result does not depend on the constant α as far as the leading asymptotic behavior is concerned.

The boundary condition at large distances is chosen as follows. Each catalyst is surrounded by a fundamental hexagonal domain of the superlattice (see Fig. 6b). Within those domains, the equilibrium is approached because of diffusion. Accordingly, the flux is zero at the boundaries between these hexagonal domains. In the original work of von Smoluchowski, the problem considered was three-dimensional, in which case these boundaries can be removed to infinity because the three-dimensional stationary solutions of (60) decays as $1/r$ with the distance r from the catalyst so that the second boundary condition may be taken as $\partial_r \sigma|_{r=\infty} = 0$ in three dimensions. However, in two dimensions, the stationary solutions grow as $\ln r$ with r so that it is not possible to obtain the reaction rate by the same considerations as in three dimensions. In two dimensions (as well as in one dimension), the problem remains non-stationary and the boundary condition must be imposed at a large but finite distance. Moreover, the hexagonal domain around one catalyst will here be approximated by a circle so that the second boundary condition used here is

$$\partial_r \sigma|_{r=L/2} = 0 \tag{62}$$

where L is the distance between two catalysts. If we suppose $\sigma \sim \exp(-2\kappa t)$, Eq. (60) becomes in two dimensions

$$\frac{d^2\sigma}{dr^2} + \frac{1}{r}\frac{d\sigma}{dr} + q^2\sigma = 0 \tag{63}$$

where $q = \sqrt{2\kappa/D}$. This is a Bessel equation, the general solution of which has the form

$$\sigma(r) = AJ_0(qr) + BY_0(qr) \tag{64}$$

in terms of the zeroth-order Bessel functions $J_0(z)$ and $Y_0(z)$.[31] Introducing (64) in (61) and (62), and taking $q \to 0$ with $L \to \infty$, we get the smallest solution as

$$q \simeq \frac{4}{L\sqrt{2\ln(2L/d)}} \tag{65}$$

so that the leading eigenvalue is

$$\kappa = \frac{1}{2} Dq^2 \simeq \frac{4D}{L^2 \ln(2L/d)} \tag{66}$$

We remark that this leading behavior is independent of the constant α of the boundary condition (61) and, hence, essentially independent of the reaction probability p_0 if L is large enough. Since $L^2 = Nd^2$, we find that the reaction rate decreases as (59) for $N \to \infty$ with a constant $C = 8$. However, since we have approximated a hexagon by a circle, we may expect that this constant is not exact. A numerical evaluation shows that the constant appearing in Eq. (59) is $C = 7.6$.

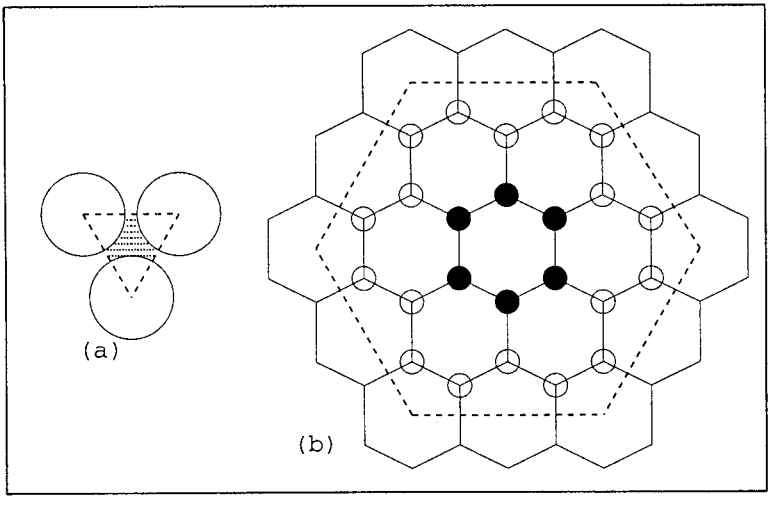

Fig. 6. (a) Triangular trap (hatched region). (b) Elementary cell in the case $n = 2$; the black dots are the reactive traps.

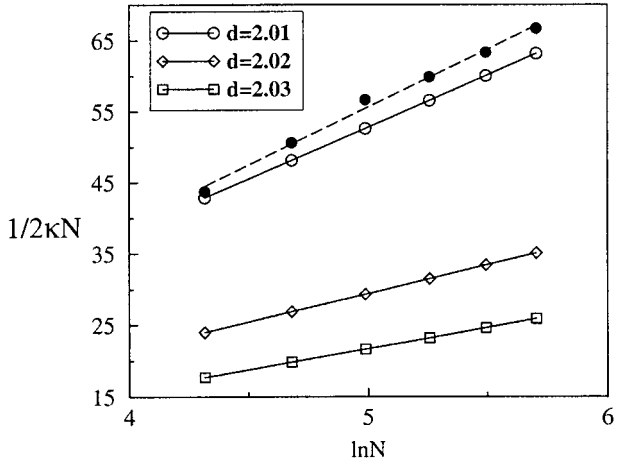

Fig. 7. Dependence of the reaction rate on N: $\kappa \sim 1/N \ln N$, for N equal to 75, 108, 147, 192, 243 and 300, and for different interdisk distances. The open symbols correspond to the random-walk model while the filled symbols are the result of the direct numerical simulations of the reactive Lorentz gas.

As can be seen in Fig. 7, the behavior $\kappa \sim 1/N \ln N$ is indeed observed for the random-walk model as well as for the reactive periodic Lorentz gas. For the reactive Lorentz gas, the reaction rate was here obtained by a direct numerical simulation of the system.

6. CONCLUSIONS

In this paper, we have studied an isomerization kinetics induced by the dynamical chaos of a periodic Lorentz gas. We have shown that the approach of the color toward the thermodynamic equilibrium can be described in terms of reactive eigenmodes corresponding to an exponential relaxation. These reactive eigenmodes are given by the eigenstates of an operator related to the Frobenius–Perron operator of the Birkhoff–Poincaré map of the Lorentz gas. This operator is obtained by two successive reductions: a spatial Fourier transform reducing the description to an elementary cell of this periodic system and a temporal Laplace transform reducing the continuous-time dynamics to the Birkhoff–Poincaré map from collision to collision. The Pollicott–Ruelle resonances associated with these eigenstates are the relaxation rates of the reactive eigenmodes. Their value at vanishing wavenumber $\mathbf{k} = 0$ gives the reaction rate κ.

The eigenstates of the Frobenius–Perron operator turn out to be distributions. Their cumulative functions have been shown to be given by

generalizations of the Lebesgue singular continuous functions. The singular character has its origin in the deterministic chaotic dynamics of the particle carrying the color. It is surprising that this singular character remains although we have assumed a reaction probability for the isomerization so that the model has an *a priori* randomness beside the dynamical randomness due to the deterministic chaotic motion of the Lorentz gas. However, this extra randomness is only assumed to occur at the surface of the phase space of the flow without modifying the deterministic equations of motion in the bulk of the phase space. For this reason, the model we consider here differs from stochastic models where randomness is assumed to occur during the motion in the bulk of the phase space.[21] For such stochastic models, we would expect the eigenmodes to be smooth. However, as we have shown here, the eigenmodes of exponential relaxation toward equilibrium remain singular for a chaotic deterministic system with an *a priori* randomness only assumed at the surface of the phase space. The singular character of the eigenstates have already been observed for diffusion,[14, 24, 25] as well as for reaction in a reactive multibaker model.[15] This singular character has its origin in the dynamical instability of the chaotic motion and appears as a corollary to the existence of the chemio-hydrodynamic modes of exponential relaxation toward equilibrium in unstable deterministic systems.

Our method allows us to obtain the dispersion relation of the reactive eigenmodes and, thus, to justify the macroscopic reaction-diffusion equations on the largest spatial scales. These reaction-diffusion equations appear with cross-diffusion terms which are small if not vanishing in the Lorentz gas. This result confirms the phenomenological treatments in which cross-diffusion is neglected.[32]

Moreover, we have analyzed the dependence of κ on the distance d between the disks as well as on the distance $L = d\sqrt{N}$ between the catalysts. This analysis reveals that, for small enough densities of catalysts, the reaction is controlled by the diffusion. With a simple random-walk model, we have obtained values of the reaction rate in good agreement with the Pollicott–Ruelle resonances of the Frobenius–Perron operator. Applying this model to different values of the density of catalysts, we have observed that the reaction rate behaves like

$$\kappa \simeq 7.6 \frac{D}{d^2 N \ln N} \tag{67}$$

where N is the number of inert disks for one catalytic disk. The behavior (67) is predicted in two dimensions by Smoluchowski's theory and confirms that the reaction is controlled by the diffusion coefficient D.

ACKNOWLEDGMENTS

We thank Professor G. Nicolis for support and encouragement in this research. The authors are financially supported by the National Fund for Scientific Research (F.N.R.S. Belgium). This work is supported, in part, by the Interuniversity Attraction Pole program of the Belgian Federal Office of Scientific, Technical and Cultural Affairs, by the Training and Mobility Program of the European Commission, and by the F.N.R.S.

REFERENCES

1. G. Nicolis and I. Prigogine, *Self-Organization in Nonequilibrium Systems* (Wiley, New York, 1977).
2. G. Ertl, *Science* **254**:1750 (1991).
3. R. Kapral, *Adv. Chem. Phys.* **48**:71 (1981).
4. M. Borkovec and B. J. Berne, *J. Phys. Chem.* **89**:3994 (1985).
5. D. C. Mattis and M. L. Glasser, *Rev. Mod. Phys.* **70**:979 (1998).
6. D. Toussaint and F. Wilczek, *J. Chem. Phys.* **78**:2642 (1983).
7. Y. Elskens, H. Frisch, and G. Nicolis, *Bull. Cl. Sci. Acad. Roy. Belg.* **69**:22 (1983).
8. Y. Elskens, H. Frisch, and G. Nicolis, *J. Stat. Phys.* **33**:317 (1983).
9. Y. Elskens and G. Nicolis, *J. Chem. Phys.* **82**:946 (1985).
10. Y. Elskens, *J. Stat. Phys.* **37**:673 (1984).
11. P. Gaspard and G. Nicolis, *Phys. Rev. Lett.* **65**:1693 (1990).
12. J. R. Dorfman and P. Gaspard, *Phys. Rev. E* **51**:28 (1995).
13. P. Gaspard and J. R. Dorfman, *Phys. Rev. E* **52**:3525 (1995).
14. P. Gaspard, *Chaos, Scattering, and Statistical Mechanics* (Cambridge University Press, Cambridge, 1998).
15. P. Gaspard and R. Klages, *Chaos* **8**:409 (1998).
16. P. Gaspard, *Physica A* **263**:315 (1999).
17. M. Pollicott, *Invent. Math.* **81**:413 (1985).
18. D. Ruelle, *Phys. Rev. Lett.* **56**:405 (1986); *J. Stat. Phys.* **44**:281 (1986).
19. L. A. Bunimovich and Ya. G. Sinai, *Commun. Math. Phys.* **78**:247, 479 (1980).
20. N. I. Chernov, *J. Stat. Phys.* **74**:11 (1994).
21. N. Wax, Editor, *Noise and Stochastic Processes* (Dover, New York, 1954).
22. G. H. Weiss, *J. Stat. Phys.* **42**:3 (1986).
23. G. P. Morriss and L. Rondoni, *J. Stat. Phys.* **75**:553 (1994).
24. P. Gaspard, *Phys. Rev. E* **53**:4379 (1996).
25. S. Tasaki and P. Gaspard, *J. Stat. Phys.* **81**:935 (1995).
26. P. Billingsley, *Ergodic Theory and Information* (Wiley, New York, 1965).
27. S. Tasaki, T. Gilbert, and J. R. Dorfman, *Chaos* **8**:424 (1998).
28. G. de Rham, *Rend. Sem. Mat. Torino* **16**:101 (1957); reprinted in *Classics on Fractals*, G. A. Edgar, ed. (Addison–Wesley, Reading MA, 1993).
29. J. Machta and R. Zwanzig, *Phys. Rev. Lett.* **50**:1959 (1983).
30. Ch. Dellago and R. Klages, *Density-Dependent Diffusion in the Periodic Lorentz Gas*, preprint (1999).
31. M. Abramowitz and I. A. Stegun, *Handbook of Mathematical Functions* (Dover, New York, 1972).
32. F. Baras and M. Malek Mansour, *Adv. Chem. Phys.* **100**:393 (1997).